JOURNAL OF COMPUTATIONAL PHYSICS 115, 390–398 (1994)

Full Wave Single and Double Scatter from Rough Surfaces

E. BAHAR AND M. EL-SHENAWEE

Department of Electrical Engineering, University of Nebraska-Lincoln, Lincoln, Nebraska 68588-0511

Received July 8, 1992; revised July 7, 1994

Using the full wave approach, the single and double scattered electromagnetic fields from deterministic one-dimensional rough surfaces are computed. Full wave expressions for the single and double scattered far fields are given in terms of multidimensional integrals. These integrals are evaluated using the Cornell National Supercomputer IBM/3090. Applying the steepest descent approximation to the double scattered field expressions, the dimensions of the integrals are reduced from four to two in the case of one-dimensional rough surfaces. It is shown that double scatter in the backward direction is significant for near normal incidence when the rough surface is highly conducting and its mean square slope is very large. Even for one-dimensional rough surfaces, depolarization occurs when the reference plane of incidence is not parallel to the local planes of incidence and scatter. A geometrical optics approximation is used to interpret the results of the double scattered fields for normal incidence near backscatter. The physical interpretation of the results could shed light on the observed fluctuations in the enhanced backscatter phenomenon as the angle of incidence increases from near normal to grazing angles. The results show that double scatter strongly depends upon the mean square slope, the conductivity of the rough surface and the angle of incidence.

I. INTRODUCTION

A full wave approach to solve problems of radio wave propagation in irregular media is used to evaluate single and double scatter from rough surfaces. The full wave expressions for the single and double scattered far fields are given in terms of multidimensional integrals. These integrals are evaluated using the Cornell National Supercomputer IBM/3090. The full wave approach is based on a complete expansion of the fields and the imposition of the exact boundary conditions at the irregular interface. The single scatter full wave expressions used here are based on a second-order iterative solution of the rigorous generalized telegraphists' equations for the scattered wave amplitudes [1–4]. The full wave solutions which satisfy reciprocity, duality, and realizability relationships in electromagnetic theory are invariant also to coordinate transformations [5].

In this work both single and double scatter are accounted for. The double scattered electromagnetic fields are evaluated from the single scattered fields that impinge upon the surface before they are rescattered to the observation point. The total scattered fields presented here are the phasor sums of the single and the double scattered fields. Thus the double scattered contributions which were previously ignored are accounted for in this work. A comparison between the single and the double scattered fields is also given here. This comparison is useful in interpreting the experimental observations conducted by Mendez and O'Donnell [6]. Mendez and O'Donnell observed strong depolarization and enhanced backscatter of light from random rough surfaces. They examined a number of theoretical approaches used in rough surface scattering but none of them account for multiple scatter.

In previous work [7], the full wave theory was used to interpret the depolarization and the enhanced backscattering of light from random rough surfaces observed in measurements conducted by Mendez and O'Donnell for oblique incidence, and the multiple scatter contributions to the total scattered fields were ignored.

In this work the full wave approach is used to evaluate double scatter (like and cross polarization) in addition to single scatter. Both self-shadowing and geometrical shadowing effects are taken into consideration.

The full wave expressions depend on the electromagnetic parameters of the media on both sides of the interface, the polarization, and the direction of the incident and the scattered waves, and the deterministically characterized rough surface height. The incident electromagnetic fields are assumed here to be plane waves.

A brief summary of the full wave approach, as well as the multidimensional integral expressions for the single and double scattered electromagnetic waves are presented in Section II. A stationary phase approximation is given in Section III. At very high frequencies, the geometrical optics method is used to interpret the results for the double scattered fields from highly conducting surfaces with large mean square slopes. Illustrative examples are given in Section IV.

II. FORMULATION OF THE PROBLEM

The interface between medium 0 and medium 1 (characterized by the complex permittivity ε_j and the permeability μ_j, $j = 0, 1$) is given by (see Fig. 1)

$$y = h(x, z). \tag{1}$$

0021-9991/94 $6.00

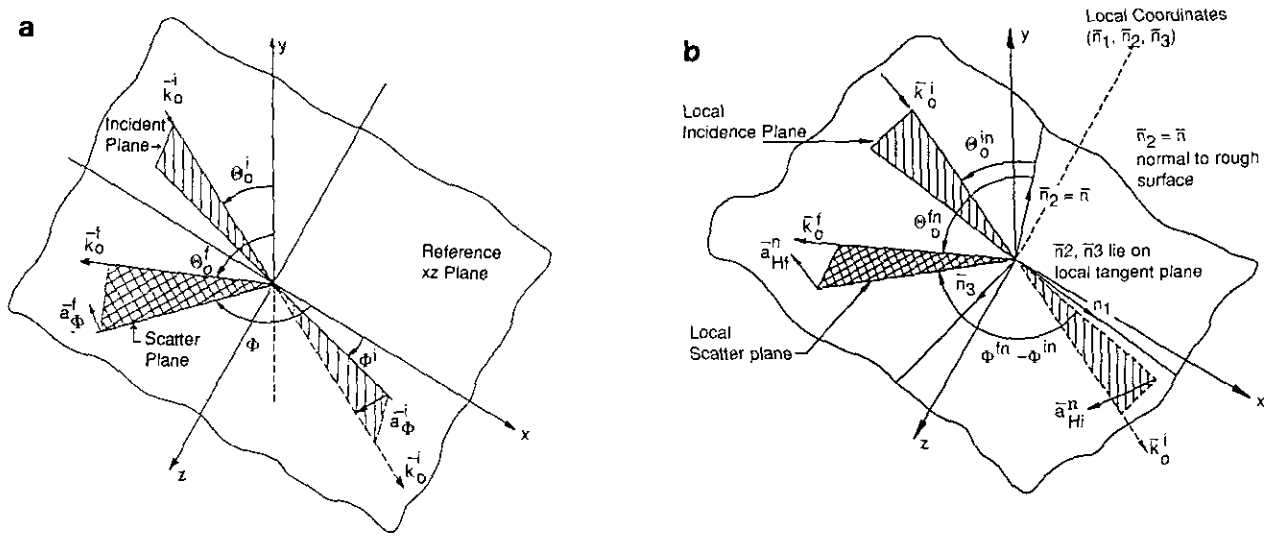

FIG. 1. (a) Plane of incidence, scattering plane, and reference x, z plane. (b) Local planes of incidence and scatter and local coordinate system.

The unit vector normal to the rough surface $f(x, y, z) = y - h(x, z) = 0$ is

$$\bar{n} = \nabla f(x, y, z)/|\nabla f(x, y, z)| = (-h_x \bar{a}_x + \bar{a}_y - h_z \bar{a}_z)/(h_x^2 + 1 + h_z^2)^{1/2}, \tag{2}$$

where $\partial h/\partial x = h_x$ and $\partial h/\partial z = h_z$. The exact boundary conditions at the rough interface are

$$[\bar{n} \times \bar{E}]_{h^-}^{h^+} = 0, \quad [\bar{n} \times \bar{H}]_{h^-}^{h^+} = 0, \tag{3}$$

where h^+ and h^- denote that the electric and magnetic fields $\bar{E}$ and $\bar{H}$, respectively, are evaluated just above and below the interface $y = h(x, z)$.

The full wave solutions for the electromagnetic fields scattered and depolarized by rough surfaces are obtained using generalized field transforms [1–4]. These generalized field transforms provide the basis for the (full wave) complete spectral expansion (in three-dimensional space) of the transverse components of the vertically and the horizontally polarized electric and magnetic fields in terms of the radiation fields, the lateral waves, and the guided surface waves of the medium [8].

On substituting the complete field expansions into Maxwell's equations for the transverse electric and magnetic field components, imposing of the exact boundary condition (3), and using the biorthogonal properties of the basis functions, the following rigorous sets of first-order coupled ordinary differential equations are obtained

$$-\frac{da^P}{dx} - ju' a^P = \sum_Q \sum_v \int (S_{PQ}^{BA} a^Q + S_{PQ}^{BB} b^Q)\, dw - A^Q \tag{4a}$$

$$-\frac{db^P}{dx} + ju' b^P = \sum_Q \sum_v \int (S_{PQ}^{AA} a^Q + S_{PQ}^{AB} b^Q)\, dw + B^Q$$

$$Q = V \text{ and } H, \quad P = V \text{ or } H. \tag{4b}$$

The symbol $\sum_v \int dw$ denotes the summation and the integration over the complete wave spectrum associated with branch cuts $\mathrm{Im}(v_o) = 0$ (radiation field), $\mathrm{Im}(v_l) = 0$ (lateral waves) and the pole of the Fresnel reflection coefficients (surface waves). The forward and backward wave amplitude are a^P and b^P, and $S_{PQ}^{\alpha\beta}$, $\alpha \neq \beta$, are the transmission scattering coefficients, $S_{PQ}^{\alpha\alpha}$, $\alpha = A$ or B, are the reflection scattering coefficients, and u' is the x-component of the wave vector $\bar{k}_j'$ in the scatter direction

$$\bar{k}_j' = k_j \bar{n}' = u' \bar{a}_x + v_j' \bar{a}_y + w' \bar{a}_z, \quad j = 0, 1. \tag{5}$$

The quantities A^Q and B^Q are the generalized transforms of the source terms.

A second-order iterative approach is used to solve the telegraphists' equations (4) for the wave amplitudes. For the suppressed $\exp(j\omega t)$ time excitation, the full wave solutions for the single scattered radiation field from a two-dimensional rough surface $f(x, y, z) = y - h(x, z)$ are given in matrix form as [9–12]

$$G^j(\bar{r}) = \left(\frac{k_0}{2\pi j}\right)^2 \int\int\int\int D(\bar{n}', \bar{n}^i)\, e^{-jk_0 \bar{n}' \cdot (\bar{r} - \bar{r}_s)}\, U(\bar{r}_s) \frac{dn_y'}{n_x'}\, dn_z' \times e^{-j\bar{k}^i \cdot \bar{r}_s}\, G^j(0) \frac{dx_s\, dz_s}{\bar{n} \cdot \bar{a}_y} \tag{6a}$$

in which $k_0 = \omega\sqrt{\mu_0 \varepsilon_0}$ is the free space wave number. The

unit vectors $\bar{n}'$ and $\bar{n}^i$ are in the directions of the scattered and incident waves:

$$\bar{n}' = (n_x' \bar{a}_x + n_y' \bar{a}_y + n_z' \bar{a}_z), \quad \bar{n}^i = (n_x^i \bar{a}_x + n_y^i \bar{a}_y) \tag{6b}$$

$$\bar{v}' = \bar{k}_0' - \bar{k}_0^i = k_0(\bar{n}' - \bar{n}^i). \tag{6c}$$

The radius vectors from the origin to the rough surface and to the observation point are $\bar{r}_s$ and $\bar{r}$, respectively, where

$$\bar{r}_s = x_s \bar{a}_x + h(x_s, z_s) \bar{a}_y + z_s \bar{a}_z, \quad \bar{r} = x \bar{a}_x + y \bar{a}_y + z \bar{a}_z. \tag{6d}$$

The shadow function $U(\bar{r}_s)$ is given by

$$U(\bar{r}_s) = \begin{cases} 1, & \text{illuminated and visible surface} \\ 0, & \textit{nonilluminated or nonvisible surface.} \end{cases} \tag{7}$$

Thus, the integrand in (6-a) vanishes for points on the rough surface which are not illuminated by the incident plane wave or visible at the observation point.

The elements of 2×1 matrices $G^i(0)$ and $G^f(\bar{r})$ are the vertically and the horizontally polarized field components (denoted by superscripts V and H, respectively) of the incident and scattered waves relative to the reference planes of incidence and scatter normal to $\bar{n}^i \times \bar{a}_y$ and $\bar{n}^f \times \bar{a}_y$, respectively (see Fig. 1),

$$G^i(0) = \begin{bmatrix} E^{Vi} \\ E^{Hi} \end{bmatrix} = \eta_0 \begin{bmatrix} H^{Vi} \\ H^{Hi} \end{bmatrix} \tag{8a}$$

$$G^f(\bar{r}) = \begin{bmatrix} E^{Vf} \\ E^{Hf} \end{bmatrix} = \eta_0 \begin{bmatrix} H^{Vf} \\ H^{Hf} \end{bmatrix} \tag{8b}$$

where $\eta_0 = \sqrt{\mu_0/\varepsilon_0}$ is the intrinsic impedance for the free space. Note that $G^i(0)$ denotes the incident plane wave at the origin while $\exp(-j\bar{k}^i \cdot \bar{r}_s)\, G^i(0) = G^i(\bar{r}_s)$ is the incident plane wave at an arbitrary point on the rough surface. The 2×2 scattering matrix $D(\bar{n}', \bar{n}^i)$ is given by

$$D(\bar{n}', \bar{n}^i) = C_0^{in}\, T^f F(\bar{n}', \bar{n}^i)\, T^i, \tag{9-a}$$

where $C_0^{in} = -\bar{n}^i \cdot \bar{n}$ is the cosine of the local angle of incidence (see Fig. 1). The elements of the 2×2 scattering matrix $F(\bar{n}', \bar{n}^i)$ depend on the polarizations and the directions of the incident and scattered waves, the unit vector $\bar{n}$ normal to the rough surface, and the electromagnetic parameters of the media on both sides of the rough interface. In general the permittivity and the permeability of medium 1, $y < h(x, z)$, can be complex to account for the dissipation of electromagnetic fields. The 2×2 scattering matrix $F(\bar{n}', \bar{n}^i)$ is given by

$$F(\bar{n}', \bar{n}^i) = \begin{bmatrix} F^{VV} & F^{VH} \\ F^{HV} & F^{HH} \end{bmatrix}. \tag{9b}$$

The matrix operator T^i transforms the waves that are vertically and horizontally polarized with respect to the reference plane of incidence (normal to $\bar{n}^i \times \bar{a}_y$) into vertically and horizontally polarized waves with respect to the local plane of incidence (normal to $\bar{n}^i \times \bar{n}$). Similarly, the matrix operator T^f transforms the waves that are vertically and horizontally polarized with respect to the local plane of scatter (normal to $\bar{n}^f \times \bar{n}$) back into vertically and horizontally polarized waves with respect to the reference plane of scatter (normal to $\bar{n}^f \times \bar{a}_y$).

The nonilluminated (self-shadow) boundary is determined by the locus of the points on the rough surface ($\bar{r}_s = \bar{r}_{s1}^i$) that satisfy

$$\bar{n}^i \cdot \bar{n}(\bar{r}_{s1}^i) = 0. \tag{10a}$$

The shadow boundary extends to the locus of points $\bar{r}_s = \bar{r}_{s2}^i$ given by

$$(\bar{r}_{s2}^i - \bar{r}_{s1}^i) \cdot \bar{n}(\bar{r}_{s1}^i) = 0. \tag{10b}$$

Similarly, the nonvisible region of the rough surface extends from the locus of points $\bar{r}_s = \bar{r}_{s1}^f$ to the locus of the points $\bar{r}_s = \bar{r}_{s2}^f$, where

$$\bar{n}^f \cdot \bar{n}(\bar{r}_{s1}^f) = 0 \tag{10c}$$

$$(\bar{r}_{s2}^f - \bar{r}_{s1}^f) \cdot \bar{n}(\bar{r}_{s1}^f) = 0. \tag{10d}$$

For a one-dimensional rough surface $h(x)$, with $\bar{n}$ in the plane of incidence, $D(\bar{n}', \bar{n}^i)$ is a diagonal matrix (no depolarization, provided that $\bar{n}^i \cdot \bar{a}_z = 0$). In this case the integration in (6a) with respect to z_s reduces to the Dirac delta function $\delta(n_z')$, where

$$\delta(n_z') = \frac{k_0}{2\pi} \int_{-\infty}^{\infty} e^{j(n_z' - 1)k_0 z_s}\, dz_s. \tag{11}$$

Thus on performing the integration with respect to n_z', the integral in (6a) reduces to

$$G^f(\bar{r}) = \frac{-k_0}{2\pi} \int\int \frac{D(\bar{n}', \bar{n}^i)}{\bar{n} \cdot \bar{a}_y} e^{-jk_0 \bar{n}' \cdot (\bar{r} - \bar{r}_s)}\, U(\bar{r}_s) \frac{dn_y'}{n_x'} \times e^{-j\bar{k}^i \cdot \bar{r}_s} G^i(0)\, dx_s, \tag{12a}$$

where for these two-dimensional field expressions

$$\bar{r}_s = x_s \bar{a}_x + h(x_s) \bar{a}_y, \quad \bar{r} = x \bar{a}_x + y \bar{a}_y. \tag{12b}$$

Assuming that $k_0 r \gg 1$, we can use the steepest descent method

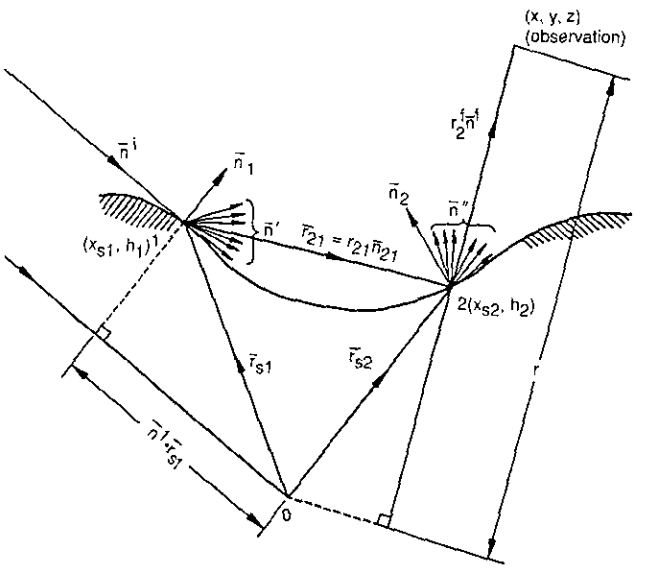

FIG. 2. The double scattered electromagnetic waves.

[13] to integrate (12a) with respect to n_y' to obtain the single scattered far fields,

$$G^f(\bar{r}) = G_0 k_0 \int \frac{D(\bar{n}^f, \bar{n}^i)}{(\bar{n}\cdot\bar{a}_y)} e^{j\bar{v}\cdot\bar{r}_s} U(\bar{r}_s)\, dx_s\, G^i(0), \qquad (13a)$$

where

$$G_0 = -e^{j\pi/4} e^{-jk_0 r}/\sqrt{2\pi k_0 r} \qquad (13b)$$

$$r = \sqrt{x^2 + y^2}, \quad \bar{v} = k_0(\bar{n}^f - \bar{n}^i). \qquad (13c)$$

The full wave expression (12) can also be used to determine the single scattered field G_2 incident upon the rough surface at $\bar{r}_{s2}$ (see Fig. 2). Thus using (12a) it follows that

$$G_2(\bar{r}_{s2}) = \frac{-k_0}{2\pi}\int\int \frac{D(\bar{n}', \bar{n}^i)}{\bar{n}_1\cdot\bar{a}_y} e^{-jk_0\bar{n}'\cdot(\bar{r}_{s2}-\bar{r}_{s1})} U(\bar{r}_{s1}) \frac{dn_y'}{n_x'} \times e^{-jk^i\cdot\bar{r}_{s1}} G^i(0)\, dx_{s1}, \qquad (14)$$

where $\bar{r}_{s1}$ and $\bar{r}_{s2}$ are the radius vectors to points 1 and 2, respectively, on the rough surface, $\bar{n}_1$ is the normal to the rough surface at $\bar{r}_s = \bar{r}_{s1}$, and $U(\bar{r}_{s1})$ is the shadow function at point 1 on the rough surface. Thus (14) can also be rewritten as

$$G_2(\bar{r}_{s2}) = \frac{-k_0}{2\pi}\int\int \frac{D(\bar{n}'\cdot\bar{n}^i)}{\bar{n}_1\cdot\bar{a}_y} e^{-jk_0\bar{n}'\cdot\bar{r}_{21}} U(\bar{r}_{s1}) \frac{dn_y'}{n_x'} \times e^{-jk_0\bar{n}^i\cdot\bar{r}_{s1}} G^i(0)\, dx_{s1}, \qquad (15a)$$

where $\bar{r}_{21}$ is the radius vector from point 1 to point 2 on the surface in the $x - y$ plane:

$$\bar{r}_{21} = (x_{s2} - x_{s1})\,\bar{a}_x + (h(x_{s2}) - h(x_{s1}))\bar{a}_y = \bar{n}_{21}\, r_{21} \qquad (15b)$$

and

$$r_{21} = \sqrt{(x_{s2} - x_{s1})^2 + (h(x_{s2}) - h(x_{s1}))^2}. \qquad (15c)$$

Assuming that $k_0 r_{21} \gg 1$, the steepest descent method can be used to integrate (15a) with respect to n_y'; thus the integrand in (15a) reduces to

$$dG_2(\bar{r}_{s2}) = \frac{-1}{\sqrt{2\pi k_0 r_{21}}} e^{j\pi/4} e^{-jk_0 r_{21}} \frac{D(\bar{n}_{21}, \bar{n}^i)}{\bar{n}_1\cdot\bar{a}_y} U(\bar{r}_{s1}) \times e^{-jk_0\bar{n}^i\cdot\bar{r}_{s1}} G^i(0)\, k_0\, dx_{s1}. \qquad (16)$$

The above expression is obviously not valid for regions where $k_0 r_{21}$ is not sufficiently large. For highly conducting surfaces it is assured that most of the incident power is scattered above the air-conductor interface. Thus the full wave solution for the double scattered fields $G_d^f(\bar{r})$ are obtained by replacing $\exp(-jk_0\,\bar{n}^i\cdot\bar{r}_s)\, G^i(0)$, the incident field at $\bar{r}_s$, in (12a) by $G_2(\bar{r}_{s2})$, see Fig. 2. It follows that

$$G_d^f(\bar{r}) = \frac{-k_0}{2\pi}\int\int \frac{D(\bar{n}'', \bar{n}^i)}{(\bar{n}_2\cdot\bar{a}_y)} e^{-jk_0\bar{n}''\cdot(\bar{r}-\bar{r}_{s2})} U(\bar{r}_{s2}) \times G_2(\bar{r}_{s2}) \frac{dn_y''}{n_x''} dx_{s2}. \qquad (17)$$

Thus,

$$G_d^f(\bar{r}) = \frac{k_0^2}{4\pi^2}\int\int\int\int \frac{D(\bar{n}'', \bar{n}')\, D(\bar{n}', \bar{n}^i)}{(\bar{n}_2\cdot\bar{a}_y)(\bar{n}_1\cdot\bar{a}_y)} U(\bar{r}_{s2})\, U(\bar{r}_{s1}) \times e^{jk_0[\bar{n}''\cdot\bar{r}_{s2} - \bar{n}'\cdot(\bar{r}_{s2}-\bar{r}_{s1})]} e^{-jk_0\bar{n}''\cdot\bar{r}} \frac{dn_y''}{n_x''}\frac{dn_y'}{n_x'} \times e^{-jk_0\bar{n}^i\cdot\bar{r}_{s1}} G^i(0)\, dx_{s1}\, dx_{s2}. \qquad (18)$$

Assuming that $k_0 r \gg 1$, we can apply the steepest descent method to integrate with respect to n_y''; thus

$$G_d^f(\bar{r}) = \frac{k_0^2}{4\pi^2}\sqrt{2\pi/k_0 r}\, e^{j\pi/4} e^{-jk_0 r}\int\int\int \frac{D(\bar{n}'', \bar{n}')\, D(\bar{n}', \bar{n}^i)}{(\bar{n}_2\cdot\bar{a}_y)\,(\bar{n}_1\cdot\bar{a}_y)} U(\bar{r}_{s2})\, U(\bar{r}_{s1}) \times e^{jk_0(\bar{n}''\cdot\bar{r}_{s2} - \bar{n}^i\cdot\bar{r}_{s1} - \bar{n}''\cdot\bar{r}_{21})} \frac{dn_y'}{n_x'} dx_{s1}\, dx_{s2}\, G^i(0), \qquad (19a)$$

where

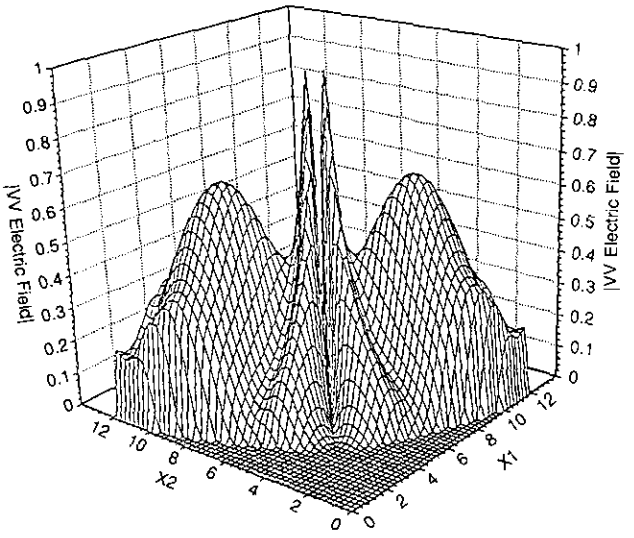

FIG. 3. Integrand of $|E^{VV}|$ for $\theta^i = 0$, $\theta^f = 0$, $\Lambda/\lambda_0 = 12.1095$, $h_0/\lambda_0 = 4.0$, $\langle h_s^2 \rangle = 2.1537$, max. slope $= 64.37°$, $\varepsilon_r = -11.43\text{-}j1.24$ (gold, $\lambda_0 = 0.633$ μm), $\mu_r = 1$.

$$r = \sqrt{x^2 + y^2}, \quad n_z'' = n_z^f = n_z^i = 0. \tag{19b}$$

Assuming that $k_0 r_{21} \gg 1$, we can apply the steepest descent method to integrate with respect to n_y^f. Thus (19) reduces to

$$G_d^f(\bar{r}) = \left(\frac{k_0}{2\pi}\right) e^{-jk_0 r} e^{j\pi/2} \int\int \frac{D(\bar{n}^f, \bar{n}_{21})\, D(\bar{n}_{21}, \bar{n}^i)}{(\bar{n}_2 \cdot \bar{a}_y)\,(\bar{n}_1 \cdot \bar{a}_y)\,\sqrt{r_{21} r}}\, U(\bar{r}_{s2})\, U(\bar{r}_{s1}) \times e^{jk_0(\bar{n}^f \cdot \bar{r}_{s2} - \bar{n}^i \cdot \bar{r}_{s1})}\, e^{-jk_0 r_{21}}\, dx_{s1}\, dx_{s2}\, G^i(0) \tag{20}$$

in which $D(\bar{n}^f, \bar{n}_{21})$ and $D(\bar{n}_{21}, \bar{n}^i)$ are evaluated at points $\bar{r}_{s2}$ and $\bar{r}_{s1}$, respectively. Even though the above approximation for the integrand is only valid when $k_0 r_{21} \gg 1$, (20) can be used to evaluate $G_d^f(\bar{r})$ instead of (19) if the scattering coefficients (9) vanish as $\bar{r}_{s2} \to \bar{r}_{s1}$ and $\bar{n}_{21} \cdot \bar{n}_1 \approx \bar{n}_{21} \cdot \bar{n}_2 \approx 0$ (see Fig. 3 in which $E^{VV} \to 0$ as $x_1 \to x_2$). In general the three-dimensional integral (19) provides more accurate results for the double scattered fields than the two-dimensional integral (20). This is discussed in detail in Section IV, where illustrative examples are presented.

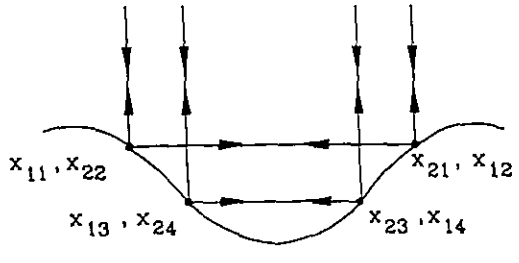

FIG. 4. Stationary phase paths for $N = 4$.

The point at $\bar{r}_{s1}$ on the rough surface should be illuminated by the incident plane wave and visible at the point $\bar{r}_{s2}$ on the surface, while the point at $\bar{r}_{s2}$ should be illuminated by a source at $\bar{r}_{s1}$ on the surface and visible at the observation point at $\bar{r}$ (see Fig. 2). Generally two sets of shadowing conditions should be satisfied. The point at $\bar{r}_{s1}$ must satisfy the shadowed conditions (10a), (10b). Thus

$$x_{s1} \leq x_1^i \quad \text{or} \quad x_{s1} \geq x_2^i \quad \text{for } \phi^i = 0 \tag{21a}$$

$$x_{s1} \geq x_1^i \quad \text{or} \quad x_{s1} \leq x_2^i \quad \text{for } \phi^i = \pi. \tag{21b}$$

Similarly, the point at $\bar{r}_{s2}$ must satisfy the shadow conditions (10c), (10d). Thus

$$x_{s2} \geq x_1^f \quad \text{or} \quad x_{s2} \leq x_2^f \quad \text{for } \phi^f = 0 \tag{21c}$$

$$x_{s2} \leq x_1^f \quad \text{or} \quad x_{s2} \geq x_2^f \quad \text{for } \phi^f = \pi. \tag{21d}$$

If the conditions (21a)–(21b) and/or (21c)–(21d) are not satisfied then $U(\bar{r}_{s1})$ and $U(\bar{r}_{s2})$ are equal to zero. The points at $\bar{r}_{s1}$ and at $\bar{r}_{s2}$ must be visible to each other.

Since the rough surface is assumed here to be one-dimensional, if $\bar{n}^i, \bar{n}^f, \bar{a}_y$, and $\bar{n}$ lie in the same plane then $\sin(\phi^{fn} - \phi^{in}) = 0$ and $F^{HV} = F^{VH} = 0$ [9]. Thus the matrices $D(\bar{n}^f, \bar{n}_{21})$ and $D(\bar{n}_{21}, \bar{n}^i)$ in (20) are diagonal.

Even though the integrand in (20) contains the term $1/\sqrt{r_{21}}$, the integrand converges smoothly to zero as $\bar{r}_{s1} \to \bar{r}_{s2}$ for finitely conducting surfaces. This is because $D(\bar{n}^f, \bar{n}_{21})$ and $D(\bar{n}_{21}, \bar{n}^i)$ vanish as $\bar{n}_{21} \cdot \bar{n}_2$ and $\bar{n}_{21} \cdot \bar{n}_1$ vanish as $\bar{r}_{s1} \to \bar{r}_{s2}$. For perfectly conducting surfaces the expression for F^{VV} does not vanish as $\bar{r}_{s1}$ approaches $\bar{r}_{s2}$. In this case the three-dimensional integral (19) is used to compute $G_d^f(\bar{r})$ for the one-dimensional rough surface.

III. GEOMETRICAL OPTICS APPROXIMATION

The geometrical optics approximation of the solution provides physical interpretation of the results. At very high frequencies the major contributions to the double scattered fields come only from the neighborhood of points 1 and 2 on the surface at which the phase $k_0\phi(x_{s1}, x_{s2})$ in the integrand (20) is stationary. The function $\phi(x_{s1}, s_{s2})$ in (20) is given by

$$\phi(x_{s1}, x_{s2}) = (\bar{n}^f \cdot \bar{r}_{s2} - \bar{n}^i \cdot \bar{r}_{s1} - r_{21}). \tag{22}$$

On differentiating $\phi(x_{s1}, x_{s2})$ with respect to x_{s1} and x_{s2}, respectively, and equating the two derivatives to zero, the solution is obtained for the pth pair of stationary phase (specular) points x_{1p}, x_{2p} (see Fig. 4). Thus in the high frequency limit the stationary phase method can be used to evaluate the double integral in (20), as [14]

$$G^f_{\text{d.Co.}} \approx K \sum_{p=1}^{N} \left\{ \left[\frac{D(\bar{n}^f, \bar{n}_{21p})}{(\bar{n}_{2p} \cdot \bar{a}_y)} e^{-jk_0 r^f_2} \right] \cdot \left[\frac{e^{-jk_0 r_{21p}}}{\sqrt{k_0 r_{21p}}} \right] \times \left[\frac{D(\bar{n}_{21p}, \bar{n}^i)}{(\bar{n}_{1p} \cdot \bar{a}_y)} e^{-jk_0 (\bar{n}^i \cdot \bar{r}_{s1p})} G^i(0) \right] \right\}, \quad p = 1, 2, 3, \ldots, N, \tag{23a}$$

where $G^f_{\text{d.Co.}}$ is the geometrical optics solution for the double scattered electromagnetic field. The subscript p defines the pth stationary phase path associated with the pth pair of specular points at $\bar{r}_{s1p}$ and $\bar{r}_{s2p}$. The normals at these points are $\bar{n}_{1p}$ and $\bar{n}_{2p}$. The distance vector between the pth pair of specular points is $\bar{r}_{21p} = \bar{r}_{s2p} - \bar{r}_{s1p} = r_{21p}\,\bar{n}_{21p}$, where $\bar{n}_{21p}$ is a unit vector. Furthermore, $r^f_2 = r - \bar{r}_{s2p} \cdot \bar{n}^f$ is the distance from point 2 on the surface to the observation point. The number of the stationary phase paths on the rough surface is N (see Fig. 4). The interference between the contributions from the different stationary phase paths results in the fluctuations in the double scattered fields. The constant K is given by [14]

$$K = \frac{-\sigma k_0}{\sqrt{|\alpha\beta - \gamma^2|}} \frac{1}{\sqrt{k_0 r}}, \tag{23b}$$

where the second derivatives α, β, and γ of $\phi(x_{s1}, x_{s2})$ are all evaluated at (x_{1p}, x_{2p}), and σ is a constant associated with α, β, and γ [14].

The diagonal elements of the matrices F (9b) reduce to the Fresnel reflection coefficients (for the vertically and horizontally polarized waves) at the pair of stationary phase points, where $\theta_0 \to \theta_0^{1p}$ and θ_0^{2p},

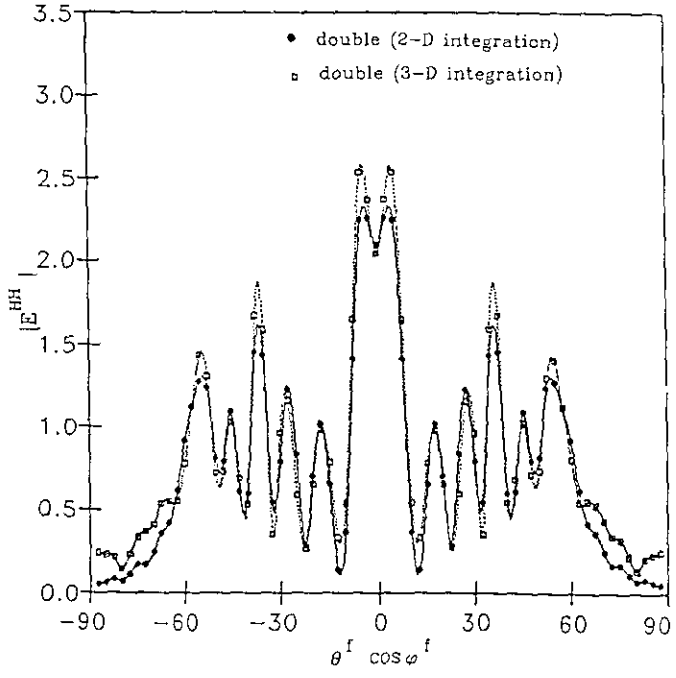

FIG. 5. $|E^{HH}|$ for $\theta^i = 0$, $\Phi^i = 0$, $\Lambda/\lambda_0 = 12.1095$, $h_0/\lambda_0 = 4.0$, $\langle h_x^2 \rangle = 2.1537$, max. slope = 64.24°, $\varepsilon_r = -11.43 - j1.24$ (gold, $\lambda_0 = 0.633\ \mu m$), $\mu_r = 1$.

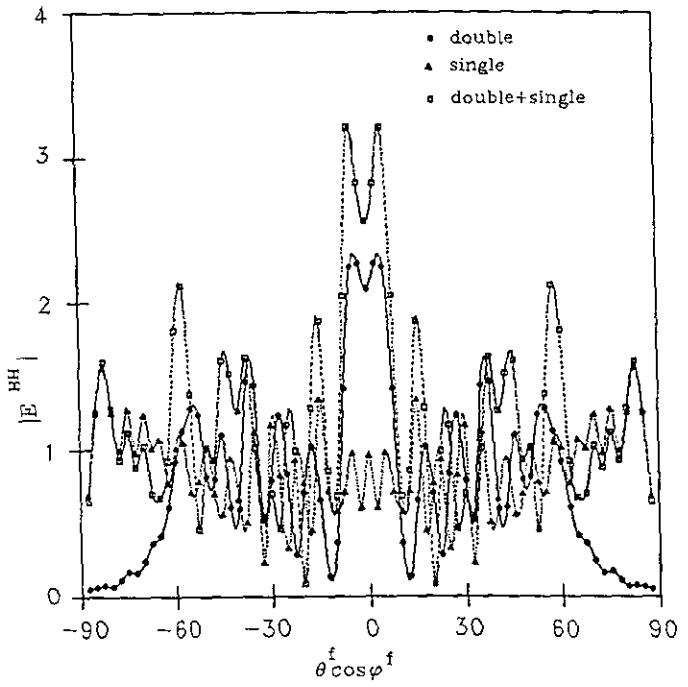

FIG. 6. $|E^{HH}|$ for $\theta^i = 0$, $\Phi^i = 0$, $\Lambda/\lambda_0 = 12.1095$, $h_0/\lambda_0 = 4.0$, $\langle h_x^2 \rangle = 2.1537$, max. slope = 64.24°, $\varepsilon_r = -11.43 - j1.24$ (gold, $\lambda_0 = 0.633\ \mu m$), $\mu_r = 1$.

$$F^{QQ}_{1p} \to R^Q_0(\theta^{1p}_0), \quad F^{QQ}_{2p} \to R^Q_0(\theta^{2p}_0), \quad Q = V, H. \tag{23c}$$

In the above derivations the stationary phase points are assumed to be isolated (the distance between pairs of specular points is larger than the wavelength). If the pairs of stationary phase points are nearby, a different asymptotic expression for the geometrical optics approximation should be used [15, 16].

IV. ILLUSTRATIVE EXAMPLES

In this section numerical examples are presented for the double scattered electromagnetic far fields. They are also compared with the single scattered electromagnetic far fields. Examples for both horizontally and vertically polarized scattered fields are given. Scattering from rough surfaces characterized by different complex permittivities and mean square slopes and heights are also computed for different incident angles. The incident excitations are assumed to be plane waves. The scattered fields are evaluated in the far zone (cylindrical waves). The rough surface is assumed to be the one-dimensional rough surface $h(x)$:

$$h(x) = h_0 \cos(2\pi x/\Lambda), \quad 0 < x < \Lambda. \tag{24}$$

The parameters h_0 and Λ are related to the mean square height $\langle h^2 \rangle = h_0^2/2$ and mean squares slopes $\langle h_x^2 \rangle = 2(\pi h_0/\Lambda)^2$. It is convenient to normalize all distances with respect to the free space wavelength λ_0.

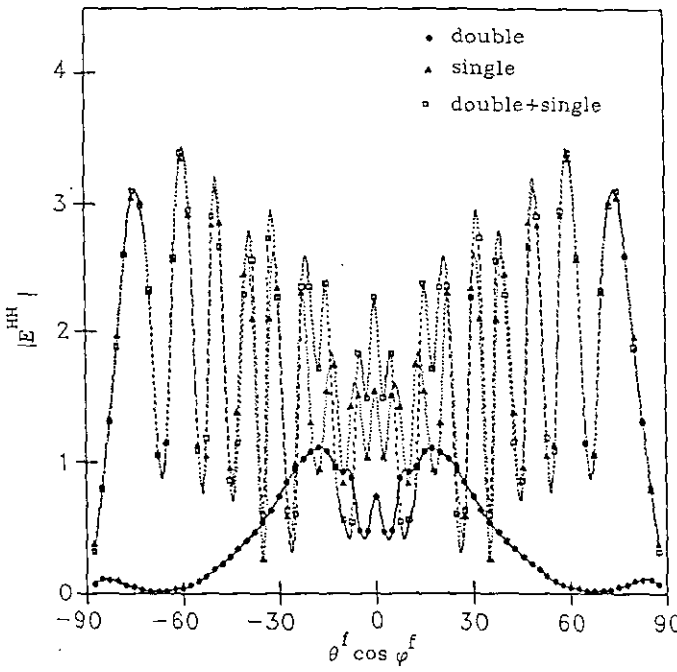

FIG. 7. $|E^{HH}|$ for $\theta^i = 0$, $\Phi^i = 0$, $\Lambda/\lambda_0 = 14.0$, $h_0/\lambda_0 = 2.0$, $\langle h_x^2 \rangle = 0.402$, max. slope = 41.9°, $\varepsilon_r = -11.43\text{-}j1.24$ (gold, $\lambda_0 = 0.633$ μm), $\mu_r = 1$.

A comparison of the double scattered fields computed by evaluating the three-dimensional integration (19) (3D) and the two-dimensional integration (20) (2D), is given in Fig. 5. The magnitude of the horizontally polarized double scattered electromagnetic fields $|E^{HH}|$ are plotted in the plane of incidence as functions of $\theta^f \cos \phi^f$ for normal incidence. The rough surface is assumed to be gold coated ($\varepsilon_r = -11.43\text{-}j1.24$ at $\lambda_0 = 0.633$ μm), $h_0/\lambda_0 = 4.0$, and $\Lambda/\lambda_0 = 12.1095$, corresponding to mean square slope $\langle h_x^2 \rangle = 2.1537$ and maximum slope 64.27°. The results show that $|E^{HH}|$ evaluated using (19) and (20) are in good agreement. Computing the two-dimensional integrals (20) using the supercomputer for backscatter at normal incidence takes about 100 cpu seconds. On the other hand, computing the three-dimensional integration (19) using the supercomputer for backscatter at normal incidence takes about 1000 cpu seconds. The program to compute the vertically polarized double scattered fields at different angles of scatter was also run using four parallel processors. Comparison of the corresponding wall-clock time and the cpu time showed a significant reduction in the wall-clock time [12, 15].

For plane wave excitations at normal incidence the fields scattered from perfectly conducting and from gold coated rough surfaces with different mean square slopes are given in Figs. 6–8. The magnitude of the horizontally polarized scattered fields $|E^{HH}|$ in the incident plane ($\phi^f = 0, \pi$) are plotted as functions of $\theta^f \cos \phi^f$. The single, the double, and the phasor sum (single + double) are shown separately in these figures. In Figs. 6 and 7, the rough surface is assumed to be gold coated ($\varepsilon_r = -11.43\text{-}j1.24$ at $\lambda_0 = 0.633$ μm) and in Fig. 8 it is assumed to be perfectly conducting. In Fig. 6 $h_0/\lambda_0 = 4$ and $\Lambda/\lambda_0 = 12.1095$; in Fig. 7 $h_0/\lambda_0 = 2$ and $\Lambda/\lambda_0 = 14.0$; in Fig. 8 $h_0/\lambda_0 = 2.3721$ and $\Lambda/\lambda_0 = 20$. The corresponding mean square slopes and maximum slopes are also given in the figures caption. Note that the double scatter fields decrease as the maximum slope of the surface decreases (Figs. 6–8). The results shown in Figs. 6–8 indicate that the horizontally polarized double scattered electromagnetic fields from highly conducting rough surfaces with large mean square slopes are significant at normal incidence near the backscatter direction. However, the like-polarized single scattered fields dominate for all scatter angles when the rough surface mean squares slopes are small, as shown in Fig. 8. When the maximum slope of the surface becomes less than 45°, $(h_x)_{\max} = 1$, the stationary phase (specular) points do not exist on the rough surface and the geometrical optics solution (23a) is not valid. The full wave solutions for the double scattered fields do not vanish for $(h_x)_{\max} < 1$. However, when pairs of stationary phase points exist (see Fig. 4), the double scatter fields are significant.

The results for the scattered fields for oblique incident angles are shown in Figs. 9 and 10. The magnitude of the vertically polarized electromagnetic scattered fields $|E^{VV}|$ are plotted in the plane of incidence ($\phi^f = 0, \pi$) as functions of $\theta^f \cos \phi^f$ (single, double, and phasor sum (single + double)). The rough surface is assumed to be gold coated ($\varepsilon_r = -11.43\text{-}j1.24$ at $\lambda_0 = 0.633$ μm) and $h_0/\lambda_0 = 4$ while $\Lambda/\lambda_0 = 12.1095$. In Fig. 9 the incident angle is $\theta^i = 45°$ and in Fig. 10, $\theta^i = 65°$.

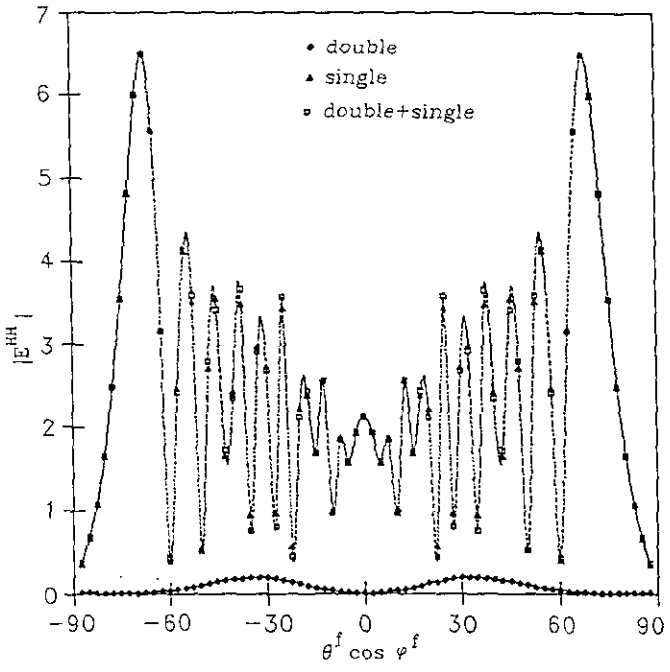

FIG. 8. $|E^{HH}|$ for $\theta^i = 0$, $\Phi^i = 0$, $\Lambda/\lambda_0 = 20.0$, $h_0/\lambda_0 = 2.3721$, $\langle h_x^2 \rangle = 0.2776$, max. slope = 36.69°, $|\varepsilon_r| \gg 1$ (perfect conductor), $\mu_r = 1$.

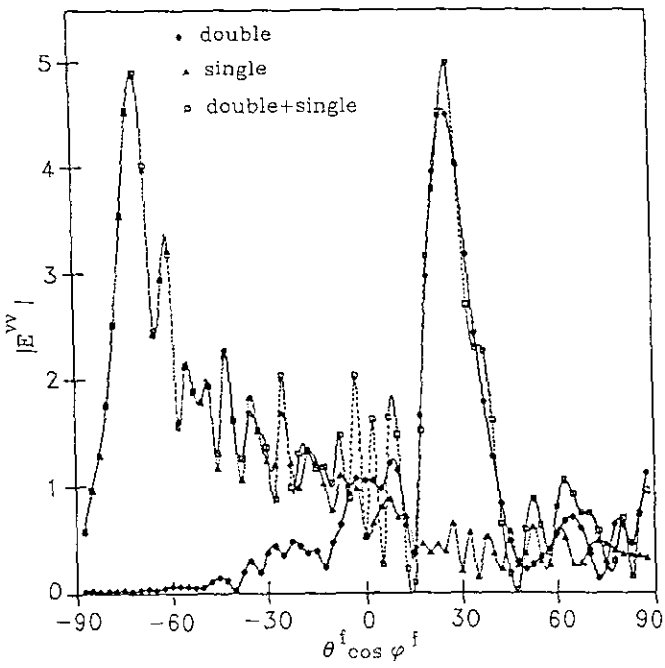

FIG. 9. $|E^{vv}|$ for $\theta^i = 45°$, $\Phi^i = 0$, $\Lambda/\lambda_0 = 12.1095$, $h_0/\lambda_0 = 4.0$, $\langle h_1^2 \rangle = 2.1537$, max. slope = 64.27°, $\varepsilon_r = -11.43\text{-}j1.24$ (gold, $\lambda_0 = 0.633$ μm), $\mu_r = 1$.

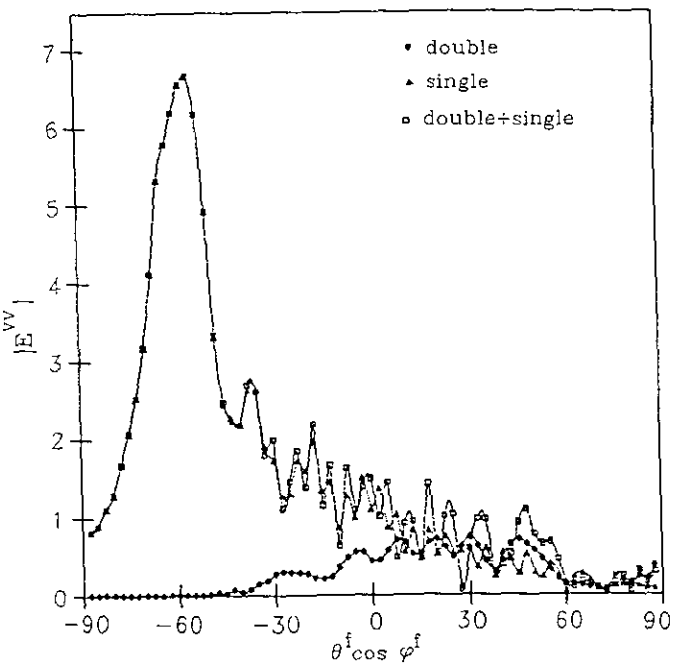

FIG. 10. $|E^{vv}|$ for $\theta^i = 65°$, $\Phi^i = 0$, $\Lambda/\lambda_0 = 12.1095$, $h_0/\lambda_0 = 4.0$, $\langle h_1^2 \rangle = 2.1537$, max. slope = 64.27°, $\varepsilon_r = -11.43\text{-}j1.24$ (gold, $\lambda_0 = 0.633$ μm), $\mu_r = 1$.

V. CONCLUDING REMARKS

Using the full-wave approach, explicit integral expressions are given for the single and the double scattered electromagnetic fields from one-dimensional (deterministic) rough surfaces. For the single scattered fields the integrals are one-dimensional. However, the double scattered fields are expressed as two- and three-dimensional integrals. Both self-shadowing and geometrical shadowing are accounted for in these expressions. The results indicate that double scatter is significant at backscatter for near normal incidence when the mean square slope is large and the rough surface is highly reflective.

At high frequencies, the major contributions of the double scattered electromagnetic fields come primarily from the neighborhood of the specular points on the rough surface (where the phase is stationary). The geometrical optics approximation can be also used to evaluate the double backscattered fields for normal incidence. These geometric optic results can only be used when the distance between the stationary phase points r_{21p} in (23a) is larger than $3\lambda_0$ [16]. The interference between field contributions from different stationary phase paths results in the fluctuations observed in the double scattered fields in the near backscatter direction for normal incidence.

For the one-dimensional rough surface the vertically polarized single scattered fields are larger than the horizontally polarized single scattered fields. However, the horizontally polarized double scattered fields are larger than the vertically polarized double scattered fields. This is consistent with energy conservation for highly reflecting surfaces [16].

Several parameters that affect the double scattered electromagnetic fields such as the mean square slope of the surface, the complex permittivities of the medium, and the angle of incidence are examined. The results of multiple scattering from realistic models of rough surfaces consisting of individual surface scatterers provide additional physical insight to the problem of multiple scattering from random rough surfaces [16, 17].

ACKNOWLEDGMENTS

The computational work was conducted at the Cornell National Supercomputer Facility supported by NSF. The research is sponsored by the U.S. Army Research Office Contract DAAL0387-K-0085.

REFERENCES

1. E. Bahar, *J. Math. Phys.* **14**(11), 1502 (1973).
2. E. Babar, *J. Math. Phys.* **14**(11), (1973).
3. E. Bahar, *Canad. J. Phys.* **50**(24), (1972).
4. E. Bahar, *Canad. J. Phys.* **50**(24), 3132 (1972).
5. E. Bahar, *IEEE Trans. Antennas Propagat.* **AP-29**(3), (1981).
6. K. A. O'Donnell and E. R. Mendez, *J. Opt. Soc. Am. A* **4**(7), (1987).
7. E. Bahar and M. A. Fitzwater, *J. Opt. Soc. Am. A* **6**(1), (1989).

8. L. M. Brekhovskikh, *Waves in Layered Media* (Academic Press, New York, 1960).

9. E. Bahar, *IEEE Trans. Antennas Propagat.* **AP-28**(1), (1980).

10. E. Bahar, *IEEE Trans. Antennas Propagat.* **AP-30**(4), (1982).

11. E. Bahar and M. El-Shenawee, "Full Wave Multiple Scattering from Rough Surfaces," in *Proceedings, IEEE International Symposium, Dallas, Texas, May 7, 1990.*

12. E. Bahar and M. El-Shenawee, "Use of Supercomputers to Evaluate Singly and Doubly Scattered Electromagnetic Fields from Routh Surfaces," in *Proceedings, Fourth Biennial IEEE Conference on Electromagnetic Fields Computation, Toronto, Canada, October 22–24, 1990.*

13. K. G. Budden, *Radio Waves in the Ionosphere* (Cambridge Univ. Press, Cambridge, UK, 1966).

14. M. Born and E. Wolf, *Principles of Optics* (Pergamon, Elmstord, NY, 1965).

15. E. Bahar and M. El-Shenawee, *IEEE Trans. Magn.* Sept., p. 4287 (1991).

16. M. El-Shenawee, Ph.D. thesis, University of Nebraska-Lincoln, August 17, 1991.

17. E. Bahar and M. El-Shenawee, "Multiple Scattering from Random Distributions of Individual Rough Surface Scatterers," in *IEEE-APS International Symposium and URSI Radio Meeting at Chicago, July 18–25, 1992.*